Descriptor Analysis in Methanol Conversion on Doped CeO_2(111): Guidelines for Selectivity Tuning

Marçal Capdevila-Cortada* and Núria López*

Institute of Chemical Research of Catalonia (ICIQ), The Barcelona Institute of Science and Technology, Av. Països Catalans, 16, 43007 Tarragona, Spain

Supporting Information

ABSTRACT: Descriptors are crucial to systematize and optimize the activity, selectivity, and stability of catalysts. Adsorption energies have usually been taken as the main representative parameters that can summarize reaction energies and activation barriers for simple reactions on relatively simple reaction sites. However, more chemically sound terms, which can be directly mapped to experiments, would be more desirable. In addition, larger molecules with more than one potentially active position and complex sites, such as the acid−base pairs present in oxides, are typically beyond the scope provided by common linear-scaling methods. In the present work, we have analyzed the selectivity of the conversion of a polyfunctional molecule on a complex oxide that presents both acid−base and redox chemistry. The conversion of methanol to formaldehyde or CO on isovalently doped ceria(111) has been taken as an example. The selectivity toward CO is triggered by the competition between formaldehyde desorption and C−H cleavage. Our results show that, by introduction of dopant cations, the activation energy of the first H stripping of formaldehyde can be decreased so that its conversion becomes favorable over desorption for Zr- and Hf-doped systems and expanded lattice ceria. More importantly, desorption is controlled by geometric and acid−base factors, whereas C−H cleavage is exclusively electronically governed through acid−base and redox factors. Thus, both geometric and electronic structure parameters are needed to optimize the performance of ceria to attain the desired selectivity. Selectivity is then estimated by a collective descriptor of the surface that incorporates the ensemble size, acid−base, and redox contributions that can be directly compared to experimental values. In addition, this scaling relationship reduces the error associated with more traditional energy-based descriptors. We anticipate that the present scheme can be extended to metal oxides and other polyfunctionalized catalysts.

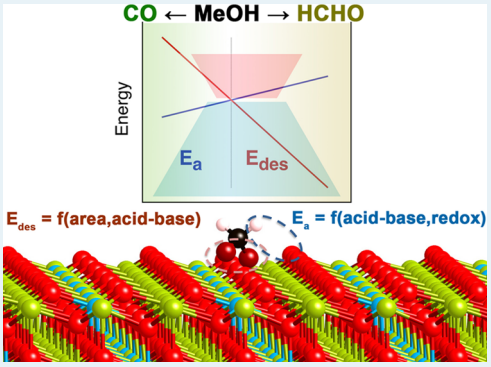

KEYWORDS: *doped ceria, scaling methods, multivariable descriptors, methanol oxidation, formaldehyde oxidation, DFT*

1. INTRODUCTION

A detailed understanding of all elementary steps that contribute to the mechanism of a given catalytic process is essential to reach a reliable rational catalyst design. From this mechanistic information it is possible to identify the crucial steps from which a set of descriptors can be extracted. The ultimate goal of obtaining these descriptors is to provide a reliable method for predicting whether a given catalyst is suitable for a specific process by using a straightforward and costless approach. The complete set of reactions might be more complex than is usually assumed, as it should include all the alternative side-product formation paths that are detrimental to performance. The obtained descriptors can then be used in large-scale predictions to seek the most suitable catalyst for the given process of interest.[1−4] Thermodynamics for adsorption can be retrieved through linear-scaling relationships by connecting adsorption energies to those of the central heteroatom of the adsorbate. This method has been reported for metals,[5] oxides, sulfide, and nitride surfaces,[6] as well as for structural defects.[7,8] However, the adsorption of large molecules such as polyalcohols on metal surfaces requires collective variables that account for the interactions both with the surface and within the adsorbate.[9] Similar multivariable descriptors were also required to generalize the adsorption of acids, esters, and ethers on metals.[10,11] Oxygen vacancy formation energy has been sometimes identified as the crucial step for oxidation processes on metal oxides,[12,13] and thus it has been the focus of studies on descriptors. Accordingly, an extensive database for oxygen vacancy formation on oxides and perovskites has been recently reported. It shows that vacancy formation follows a collective variable that contains bond strength and electronic structure data.[14,15]

Kinetic parameters can also be obtained through the use of descriptors. The Brønsted−Evans−Polanyi (BEP) relationships state that, when a group of transition states are similar in nature, a change in the thermodynamics of the reaction, ΔE, is proportionally accompanied by a change in the kinetics and hence the activation energy, E_a, of this reaction.[16,17] From this

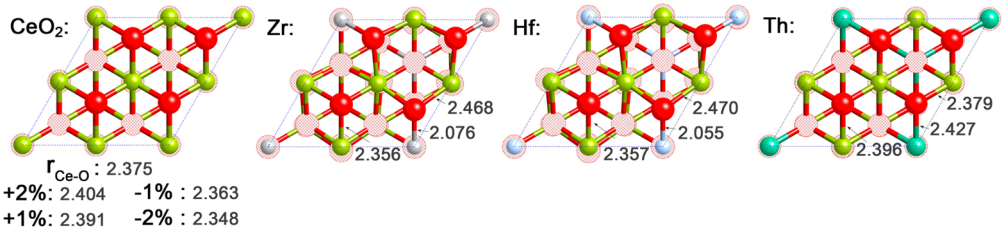

Figure 1. Top view of the (111) facet for undoped CeO_2, and Zr-, Hf-, and Th-doped CeO_2. Nonequivalent distances are shown in Å. The outmost oxygen (in red), cerium (in light green), and dopant (Zr in silver gray, Hf in blue, and Th in dark green) layers are highlighted, while the rest of the atoms are shown dashed.

early proposal as a starting point, several alternative formulations that end up correlating with a single adsorption energy have been derived.[18−23] In particular, the transition state scaling (TSS) relationships correlate the transition state energy with the energy of the initial or the final state of the reaction.

Among oxides, CeO_2 constitutes a unique catalytic system:[24] although it is based on a rare-earth metal, it is relatively abundant and cheap and can be easily doped. This material presents a significant charge separation and a surface acid and basic character. Moreover, cerium cations easily cycle between the Ce(IV) and Ce(III) oxidation states, rendering a low vacancy formation energy.[25] This feature, together with easy bulk transport, allows ceria to release or absorb oxygen under reducing or oxidizing conditions, a phenomenon commonly known as oxygen storage capacity.[26] As a consequence, ceria has a prominent role in oxidations, either as a catalyst or as a support in reactions including the water-gas shift (WGS),[27,28] SO_2 oxidation,[29,30] and the Deacon process.[31] In addition, cerium oxide also presents high activity and selectivity in hydrogenations.[32]

Several of the ceria catalytic properties can be improved by using dopants.[33] Low-valence dopants induce long-range effects, whereas tetravalent dopants mostly produce local effects.[34] Among all dopants, tetravalent ions do not imply a major change in the electronic structure but only a structural change, the impact of which will depend on the dopant atomic radius and its concentration. Trivalent cations (e.g., Sm, Gd, La, and Y) increase the ionic conductivity of ceria,[35−38] thus improving the performance for use in solid oxide fuel cells.[39] Ionic conductivity and oxygen vacancy formation on doped ceria have been extensively analyzed using density functional theory (DFT).[40−49] Another trivalent dopant, Ga, enhances the activity of alkyne semihydrogenation,[50] and Zr, Hf, Pd, or Cu impurities improve the catalytic activity of the WGS[51,52] and PROX[53,54] reactions. On the other hand, isovalent Hf and Zr dopants enhance the catalytic activity in the Deacon process in comparison to trivalent dopants, even if it is an oxidation reaction (HCl).[55] Other processes such as NO_2 reduction,[56] NH_3 oxidation,[57] and CO_2 methanation[58−60] have also been computationally analyzed.

The present study focuses on the catalytic conversion of methanol on doped ceria(111) to formaldehyde and CO. The conversion of methanol is considered an ideal test for characterizing the catalytic behavior of metal oxides, as it entails acid−base and redox steps[61,62] while being one of the smallest possible surrogates for a large class of biomass-derived compounds. Methanol decomposition is structure sensitive and produces formaldehyde on CeO_2(111) and CO/H_2 on the (100) facet,[63,64] due to the competition between C−H cleavage in formaldehyde in comparison to its desorption.[65] In the present work, we have used DFT+U on geometrically modified CeO_2(111) surfaces, either by isovalent doping or by applying strain. The selectivity toward CO was analyzed through chemical descriptors that demonstrate the complex balance of geometric and acid−base contributions in the adsorption of formaldehyde and redox and acid−base properties in C−H activation. Our results point out the relevance of chemical descriptors that can be directly mapped to experimentally derived properties and, when appropriately combined, provide a more accurate representation than traditional BEP and TSS methodologies.

2. COMPUTATIONAL DETAILS

All calculations were performed at the DFT+U level using the Vienna ab initio simulation package (VASP, version 5.3.3),[66,67] with the Perdew−Becke−Ernzerhof (PBE)[68] functional. The self-interaction error was diminished by the addition of an effective Hubbard U term, following the approach of Dudarev et al.[69] This U_{eff} value was set to 4.5 eV, as it was been previously proven to provide satisfactory results.[55,70−72] Projector-augmented wave (PAW) pseudopotentials[73] were used to describe the core electrons with a plane-wave cutoff energy of 500 eV for the valence electrons (i.e., 5s, 5p, 4f, 6s for Ce atoms, 2s, 2p for O and C atoms, 4s, 4p, 5s, 4d for Zr atoms, 5s, 5p, 6s, 5d for Hf atoms, and 6s, 6p, 5f, 7s for Th atoms).

Ceria presents a fluorite structure, with a lattice parameter of a_{exp} = 5.411 Å.[74] The lattice parameter was optimized using a dense Γ-centered 7 × 7 × 7 k-point mesh that leads to a value of a_{calc} = 5.497 Å, in good agreement with both the experimental value and previous computational studies.[75] The (111) surface was modeled as $p(2 \times 2)$ with periodically repeated slabs consisting of three O−Ce−O layers separated by 15 Å of vacuum space, which was optimized using a Γ-centered 3 × 3 × 1 k-point mesh. The five outermost single layers and the adsorbates were allowed to relax, whereas the rest of the atoms were kept fixed to their bulk positions. Doped (111) slabs of $Ce_{0.75}M_{0.25}O_2$, where M = Zr, Hf, Th, were obtained by substituting one cerium atom for one dopant M atom in the bulk structure's unit cell. For the description of Th atoms, an effective U term, U_{eff}, of 4.5 eV was also used. The doped bulk structures were then optimized as specified before (the resulting lattice parameters are $a_{calc,Zr}$ = 5.404 Å, $a_{calc,Hf}$ = 5.394 Å, and $a_{calc,Th}$ = 5.544 Å), and the slabs were built likewise. Alternatively a lattice strain was applied to the surface slab on the two periodic dimensions (x and y). Strains of 1% and 2% expansions and contractions were performed. Density of states (DOS) calculations were obtained using a denser Γ-centered 13 × 13 × 1 k-point mesh.

Transition states were located by means of the climbing image nudged elastic band (CI-NEB) method.[76] In some

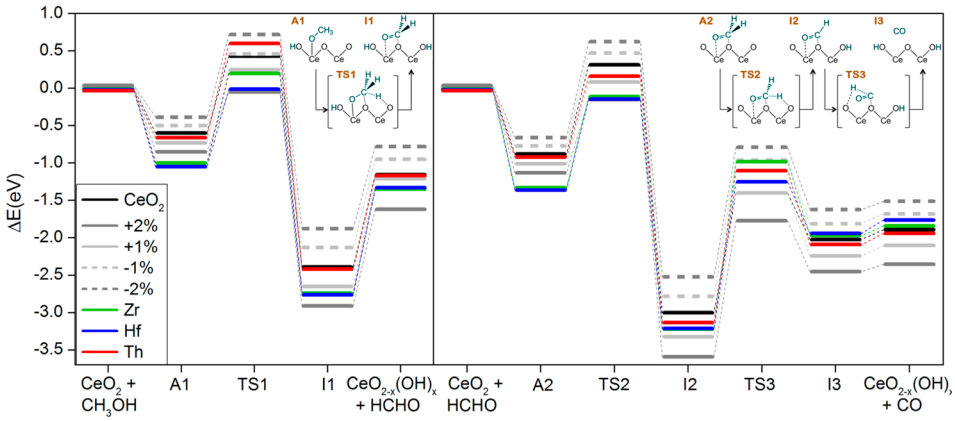

Figure 2. Energy profiles for the conversion of (left) methanol to formaldehyde and (right) formaldehyde to CO upon adsorption on pristine and doped ceria(111). All relative energies are collected in Table S1 in the Supporting Information. Inset: schematic representation of all intermediates and transition states involved in each process.

particular cases, the CI-NEB was complemented by the improved dimer method (IDM).[77] The nature of all reaction minima and transition states was confirmed by performing numerical frequency analyses (step size ±0.01 Å).

3. RESULTS AND DISCUSSION

3.1. Structural Analysis. The doping of the CeO_2(111) facet has been addressed through two strategies. The bulk structure was optimized with 25% concentration of dopant, namely Zr, Hf, and Th, in order to evaluate the effects brought about by structural variations and the direct impact of dopant−adsorbate interactions. Additionally, 1% and 2% expansion and contraction strains were also applied to the undoped bulk structure to assess the sole effects triggered by structural variation. Zr- and Hf-doped ceria induce contraction to the unit cell (1.69 and 1.87%, respectively), whereas Th-doped ceria expands the cell by 0.86%. Upon doping, surface Ce−O distances do not increase or decrease evenly, as shown in Figure 1. These distances involving oxygens only surrounded by Ce atoms slightly decrease (increase) after doping that induces cell contraction (expansion). The other lattice O atoms are surrounded by two Ce atoms and the dopant, where the Ce−O distances greatly increase on Zr and Hf doping, while they only slightly increase on Th-CeO_2. The M−O distances, where M is the dopant, increase for Th−O in comparison to Ce−O, whereas they drastically decrease for Zr−O and Hf−O. It is worth noting that explicit doping with smaller ionic radius dopants, despite the overall lattice contraction, induces certain surface motifs with effective expansion.

The electronic structure, analyzed through the band structure and density of states (DOS), is also altered upon doping. In particular, the projected DOS (PDOS) of the O(2p) band corresponding to lattice oxygens is shifted from the Fermi level reference (Figure S1 in the Supporting Information). The center of the O(2p) band is shifted toward lower (more stable) energies for all explicitly doped surfaces: −119, −223, and −100 meV for Zr-, Hf-, and Th-CeO_2. Contraction also shows a −104 (1%) to −119 meV (2%) O(2p) band shift, while expanded ceria shifts 51 and 54 meV toward higher energies for 1% and 2% expansions. This fact is directly related to the acid−base character and therefore activity of the surface.

3.2. Reactivity. The conversion of methanol to formaldehyde and CO was investigated on the (111) facet of ceria for all aforementioned doping strategies and compared to the reactions on the undoped facet (Figure 2). The reaction mechanism for methanol conversion to formaldehyde consists of the steps

$$CH_3OH + 2^* \rightarrow CH_3O^* + H^* \quad (R1)$$

$$CH_3O^* + ^* \rightarrow HCHO^* + H^* \quad (R2)$$

$$HCHO^* \rightarrow HCHO + ^* \quad (R3)$$

Methanol adsorbs on ceria dissociatively and leads to a chemisorbed methoxy group and a surface hydroxyl (R1). This first step occurs in a dual acid−base site, formed by an accessible Ce(IV) and a lattice oxygen.[61] This is followed by a C−H cleavage that conducts to chemisorbed formaldehyde and another surface hydroxyl group (R2). This process entails a redox step, where the methoxy is oxidized and two surface Ce(IV) are reduced to Ce(III). The methoxy is partially reduced in the associated transition state, leading to a radicaloid species, where one electron is delocalized over the C, H, and the surface O, and one single Ce(IV) is reduced to Ce(III), as noted also in ceria and other reducible oxides.[65,78−80] In the final step, formaldehyde desorbs from the surface to the gas phase (R3). For ceria(111), the barrier for the C−H bond breaking is 1.03 eV and the reaction is exothermic by 1.78 eV.[65,78] The resulting chemisorbed HCHO binds rather strongly, 1.23 eV, therefore allowing an eventual subsequent conversion to CO.

The doped facets present two major sites, depending on whether the adsorbate's oxygen interacts with the surface dopant (M···O) or cerium (Ce···O). Since methanol adsorption is 0.2 eV larger on the M···O site, the reaction was only considered there. Doped Zr-CeO_2 and Hf-CeO_2 enhance the dissociative adsorption of methanol. The next step, C−H cleavage, presents energy barriers of 1.04 and 1.19 eV, respectively, similar to the undoped values. The transition states exhibit the same nature as on the pristine surface. On the other hand, the adsorption energies of all intermediates on Th-CeO_2 are almost identical with those on the pristine surface, whereas the activation energy for the C−H bond breaking is 0.23 eV higher. The results on the doped surfaces are in contrast with those obtained after applying strain to the pristine lattice. Despite the lattice contraction caused by Zr and Hf doping, an even contraction hinders this particular reaction. In contrast, lattice expansion favors the reaction, since the energy barrier for the C−H cleavage is only 0.80 eV for +2% and the

reaction energy is 0.3 eV higher than those on the undoped and the doped facets. The results obtained on the doped facets are in good agreement with the surface distribution depicted in Figure 1, where Zr-CeO_2 and Hf-CeO_2 exhibit motifs of effective Ce−O expansion.

The conversion of formaldehyde to CO on ceria (111) comprises the elementary steps

$$HCHO + * \rightarrow HCHO* \quad (R3')$$

$$HCHO* + * \rightarrow CHO* + H* \quad (R4)$$

$$CHO* + * \rightarrow CO* + H* \quad (R5)$$

$$CO* \rightarrow CO + * \quad (R6)$$

Formaldehyde chemisorbs on ceria (R3′). This is the reverse process of the last step of the previous reaction (R3). Upon adsorption, formaldehyde suffers a C−H bond breaking that leads to chemisorbed CHO and a surface hydroxyl through an overall redox step (R4), where again two surface cerium cations are reduced to Ce(III). The transition state also involves the reduction of one Ce(IV) to Ce(III), where the other electron is delocalized over the C, H, and the surface oxygen.[65] This is followed by a second C−H cleavage that results in physisorbed CO and a second surface hydroxyl group (R5). Finally, CO desorbs from the partially hydroxylated surface to the gas phase (R6). On the undoped facet, the energy barrier for formaldehyde C−H cleavage is 1.19 eV. This process is 0.32 eV more demanding than formaldehyde desorption, and this fact is ultimately responsible for the experimentally observed formaldehyde selectivity.[65] Then, the energy required for the second C−H stripping is 1.60 eV, through an endothermic reaction of 0.98 eV. The final CO desorption only demands 0.13 eV.

The adsorption of formaldehyde on Zr-CeO_2(111) and Hf-CeO_2(111) is 0.5 eV stronger than that on the undoped facet. It presents binding energies of −1.33 and −1.36 eV, respectively (Figure 2). For HCHO conversion, the M···O site was also considered, since it is the starting point after methanol conversion and this site is 0.4 eV more stable than the Ce···O site. The energy barrier to C−H bond breaking is 1.22 eV on both doped facets, similar to the case for the undoped surface. However, given the high binding energy of formaldehyde in these doped surfaces, C−H cleavage requires 0.11 (Zr) and 0.15 eV (Hf) less energy than HCHO desorption and therefore both processes will compete. Th-CeO_2 exhibits values similar to those of the undoped surface for the adsorption and the first C−H stripping. The reaction then proceeds with similar adsorption energies for **I2** and CO on the three doped and the undoped facets. The energy barrier of the second C−H cleavage increases for the three doped surfaces in comparison to the undoped surface, increasing up to 2.0 eV for Zr- and Th-CeO_2 and to 2.2 eV for Hf-CeO_2. Similar to what was observed for the methanol conversion to formaldehyde, lattice contraction exhibits lower binding energies of all intermediates and higher energy barriers and thus impedes the decomposition of formaldehyde to CO. All intermediates, in contrast, bind more tightly on the expanded lattice. The first C−H cleavage requires 0.4 eV less energy on +2% than on pristine CeO_2, whereas the second H stripping demands 0.2 eV more energy. On this expanded surface, formaldehyde desorption is 1.13 eV and the energy barrier for its first C−H bond breaking is 0.98 eV, hence enabling the conversion of formaldehyde to CO.

Therefore, the use of dopants (Zr, Hf) allows modifying the selectivity of the most stable facet of ceria for the particular process of methanol conversion. Whereas pristine ceria(111) converts methanol to formaldehyde, Zr-CeO_2 and Hf-CeO_2 allow its evolution to CO, which would help to enable the concomitant production of syngas (CO + H_2). Moreover, an even lattice expansion also allows the conversion of methanol to CO. This would be the case, for instance, of a rather high concentration of subsurface doping using dopants larger than cerium.

4. DESCRIPTOR ANALYSIS

The correlation between thermodynamics and kinetics can be assessed by means of the Brønsted−Evans−Polanyi (BEP) and the transition state scaling (TSS) relationships, as we stated in the Introduction. The BEP and TSS relationships for the selectivity-determining step of this reaction, i.e. the first C−H cleavage of formaldehyde, are shown in Figure 3. Although the standard BEP correlating E_a and ΔE provides a reasonable description of this process, the correlation is improved when E_{TS} is presented as a function of the initial state energy E_{IS}. This result is in good agreement with the exothermic nature of the reaction and the similar geometries of the initial and transition states.

The individual deviations from some of the points obtained through the BEP and TSS relationships are, however, exceedingly large for a sufficiently accurate prediction. For instance, in the BEP activation energies with an 0.05 eV span (topmost points) correspond to reaction energies ranging from −2.12 to −1.84 eV. Similarly, on both TSS Zr- and Hf-CeO_2 present E_{TS} values close to the +2% result, whereas their E_{IS} and E_{FS} values differ by 0.20 and 0.35 eV, respectively. In addition, for the TSS relationships, strained CeO_2 and Th-CeO_2 exhibit a visible linear correlation (red lines), although the trend is not followed by Zr- and Hf-CeO_2 (blue lines). The ultimate consequence is that the overall fittings are reasonable but the predictions on different areas of the graphs are affected by errors that can amount up to 0.21 eV, which limits the predictive power of the BEP and TSS for the individual points. It is worth pointing out that BEP and TSS relationships allow energy-based predictions, which are a useful tool for computations but are not so straightforward to obtain from experiments.

Adsorption and reactivity are usually described in terms of geometric and electronic contributions.[81] In the following, we try to incorporate descriptors that encompass these terms, thus extending the electronic structure analysis on the metal d-band center to more complex multifunctional surfaces.[82] The concepts behind our formulation have been qualitatively described, but to date they lack a complete, physically sound quantification. Grasselli suggested seven pillars that govern selectivity in heterogeneous oxidation catalysis:[83] host structure, metal−oxygen (M−O) bond, lattice oxygen, redox, multifunctionality of active sites, site isolation, and phase cooperation. Inspired by these fundamental pillars, we have developed a set of descriptors that have been employed to describe the two steps that trigger the selectivity of methanol conversion to CO: i.e. formaldehyde desorption and HCHO first C−H stripping. Our set of descriptors include the following.

(a) Ensemble area, *A*, which accounts for the host structure in Grasselli's nomenclature. In particular, we considered the

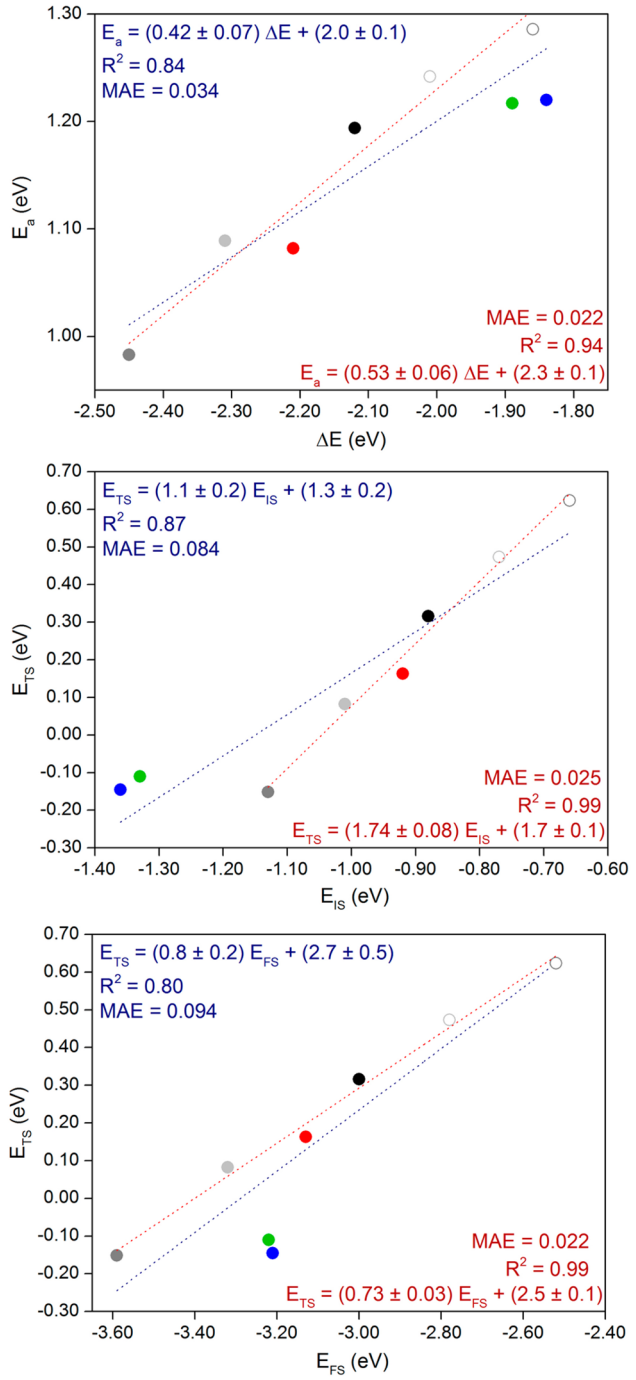

Figure 3. (top) Brønsted–Evans–Polanyi (BEP) and (bottom) transition state scaling (TSS) relationships for the first C–H cleavage of formaldehyde. The fittings were done in two different ways: including all the points (blue) and excluding Zr and Hf (red). MAEs are given in eV.

area comprised in the triangle formed by three lattice oxygens (Figure S2 in the Supporting Information).

(b) Lattice parameter, *a*, which would be equivalent to the host structure in Grasselli's formulation. It is a direct consequence of the expansion or contraction introduced by doping.

(c) M–O distance, r_{M-O}, accounting for the M–O bond in Grasselli's formulation. This is obtained as the mean value of the three M–O distances of the oxygen of interest, where M is either Ce or the dopant.

(d) Basicity of lattice oxygens, O(2p), equivalent to Grasselli's lattice oxygen. This term is obtained as the center weighted average in the PDOS of the O(2p) band.

(e) Redox character, red, which refers to Grasselli's redox. It is estimated to be the energy difference between the surface and the reduced surface upon the addition of one electron, with the concomitant reduction of one Ce(IV) to Ce(III), after relaxation.[84]

Grasselli's site isolation would be required to analyze possible condensation routes in methanol conversion,[85] but it does not apply to the present analysis. Similarly, phase cooperation does not contribute either, due to the stability of the CeO_2 phase in comparison to other methanol conversion catalysts such as MoO_x.[86,87]

In summary, we consider three geometric (i.e., ensemble area, M–O distance, and lattice parameter) and two electronic (i.e., basicity and redox) descriptors. The values for all of these parameters for all the surfaces in the study are collected in Table S2 in the Supporting Information. Geometric descriptors have provided important insights in describing the adsorption and dissociation of CO on metal surfaces.[88,89] Acid–base properties have been shown to control adsorption and reactions on metal oxides[90] and metals,[91] whereas the redox character controls the conversion of methanol to formaldehyde on vanadia supported on ceria.[12,79] It is worth noting that these properties are easily accessible. Geometric parameters can be obtained by performing a simple calculation on the optimized cell and can be derived experimentally from the XRD data or more accurately from adsorption measurements (BET). The acid–base character can be experimentally measured by the adsorption of probe molecules (CO or NH_3), monitored through FTIR spectroscopy,[92] whereas the redox properties can be investigated experimentally by temperature-programmed reduction (TPR) or oxygen isotopic exchange.[93]

The performance of these five descriptors has been evaluated for the two competing steps: formaldehyde desorption energies, E_{des}, and the C–H activation barriers, E_a (see Figures S3 and S4 in the Supporting Information). Among all the individual descriptors, E_{des} only correlates well with the ensemble area. The rationale behind this is that a larger ensemble area permits a better accommodation of chemisorbed formaldehyde, thus increasing its desorption energy. The same magnitude, however, does not describe the activation energy for the next step. For C–H stripping, three of the descriptors, redox character, lattice parameter, and the M–O distance, provide a relevant correlation. This is due to the fact that the transition state **TS2** encompasses the reduction of a surface Ce(IV) to Ce(III), and since the Ce(III) cation is larger than Ce(IV), it is stabilized in larger cells. The other descriptors considered are unable to correlate either the formaldehyde desorption energy or the activation energy of its first C–H cleavage. Although these descriptors are based on fairly accessible properties of the catalyst, they do not actually improve the previous results provided by the BEP and TSS relationships.

As some of the steps seem to have a mixed component, two-variable descriptors were then investigated. Formaldehyde chemisorbs on a lattice oxygen, forming an O–C bond, and the first C–H stripping forms a surface hydroxyl, suggesting that oxygen basicity may be relevant on both steps. Thus, our collective descriptors embrace the main descriptor previously identified together with the corresponding oxygen basicity. As can be seen, this approach provides a notable improvement on both correlations (see Figure 4). Hence, the basicity of lattice

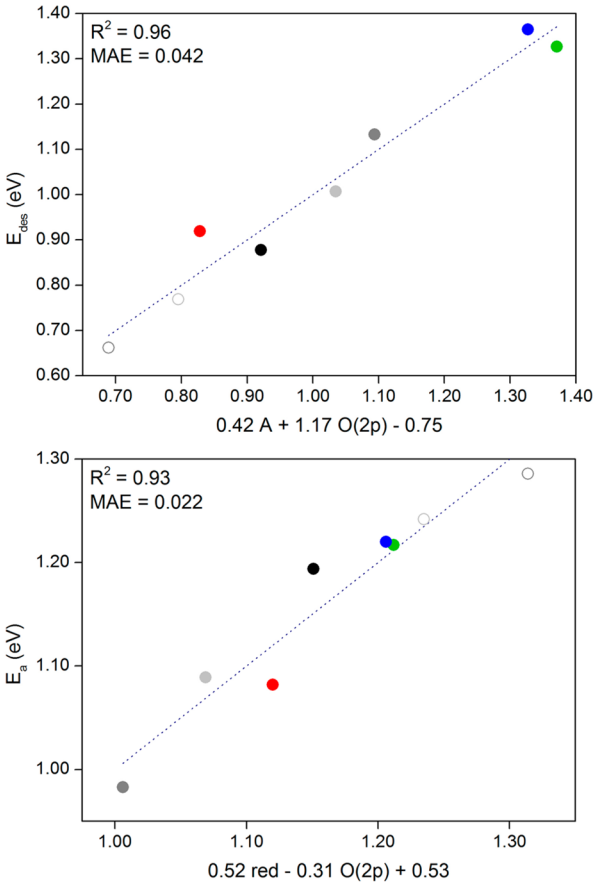

Figure 4. (top) E_{des} and (bottom) E_a as a function of a two-variable descriptor, embracing the site area and oxygen basicity for formaldehyde desorption and the redox character and oxygen basicity for the first C−H cleavage.

oxygens plays a prominent role in both steps, despite not being able to correlate any of these magnitudes as a single descriptor. The two-variable description improves the previous scaling methods, halving the mean absolute errors (MAE). Furthermore, this approach naturally includes Zr- and Hf-CeO_2, which were outliers in the BEP and TSS relationships. The collective descriptor including the redox character provided a better result than that with the lattice parameter or the M−O bond, although they also improved the correlation yielded by the single-variable descriptor (Figure S5 in the Supporting Information). It is finally worth noting that these two-variable descriptors accurately represent Grasselli's multifunctionality of the active sites.

To summarize, formaldehyde desorption energy is described as a sum of ensemble area and basicity contributions and its first C−H cleavage activation energy as a sum of redox and basicity contributions:

$$E_{des} = \alpha A + \beta[\mathrm{O(2p)}] + \zeta \quad (1)$$

$$E_a = \delta[\mathrm{red}] + \gamma[\mathrm{O(2p)}] + \lambda \quad (2)$$

As mentioned before, the competition between these two steps triggers the selectivity in methanol conversion. Given the definition of E_a, these two variables are related by the transition state energy E_{TS}:

$$E_a = E_{TS} - E_{IS} = E_{TS} + E_{des} \quad (3)$$

Hence, the energy of the transition state for the C−H stripping is the value that ultimately determines selectivity: positive E_{TS} translates to $E_a > E_{des}$ (i.e., MeOH reacts toward HCHO), whereas a negative value implies $E_a < E_{des}$ (i.e., MeOH converts into CO). Substitution of eqs 1 and 2 into eq 3 results in a general description of E_{TS} based on our previous findings:

$$E_{TS} = \delta[\mathrm{red}] - \alpha A + (\gamma - \beta)[\mathrm{O(2p)}] + (\lambda - \zeta) \quad (4)$$

The values previously obtained fitting the two-variable descriptors on eqs 1 and 2 can be introduced in eq 4 (Figure 5). Our results manifest a clear improvement in comparison to

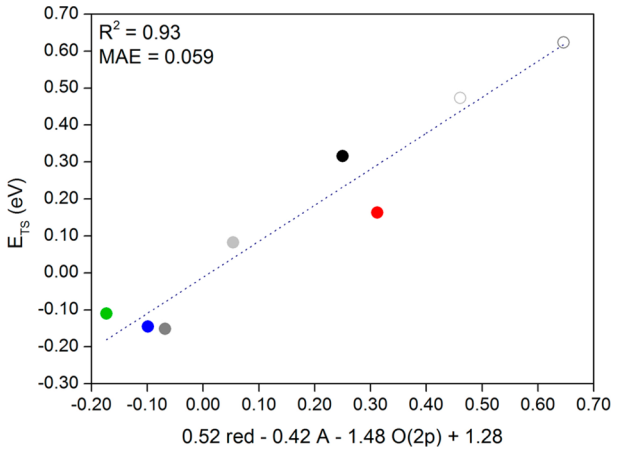

Figure 5. E_{TS} as a function of a three-variable descriptor, embracing redox, site area, and oxygen basicity, based on eq 4 and the previous fitted relations.

the TSS relationships, which also provided a prediction for E_{TS}. This is seen in the individual errors and the MAE. The ultimate consequence is that the present results reduce the errors by more than 0.1 eV, thus improving the predictive power of the scaling relationships. For instance, this error reduction would lead to the improvement of predicted rates by 1 order of magnitude (for a reaction at 500 K).

5. CONCLUSIONS

In the present work, a thorough analysis of potential descriptors for the chemistry on oxides has been carried out focusing on the selective dehydrogenation of methanol on doped ceria(111), by means of density functional theory. This methodology can help to assign these effects in a structured manner and to upgrade wide concepts such as acidity, basicity, ensemble, and redox to descriptors that can be mapped to calculated quantities and/or experiments with probe molecules. To prove the principle, we took methanol decomposition on the pristine surface, where methanol selectively converts to formaldehyde due to the high activation energy for its first C−H cleavage in comparison to its desorption. In contrast, we showed that, when properly doped, the final product can be CO. For this mechanism we compared the traditional BEP and TSS linear relationships to the performance of newly defined descriptors that summarize three geometric and two electronic parameters that can be directly mapped to experiments. Our work evidences the difficulties of adaptability of BEP and TSS relationships and single descriptors to explain the complexity of multifunctionalized intermediates and mixed sites on the surfaces. BEP and TSS are still able to provide rather acceptable

correlations, but the associated individual errors can exceed 0.1 eV; in addition, there is a notable underperformance for doped Zr- and Hf-CeO_2 in comparison to the rest of the surfaces. Instead, with the chemical descriptors, formaldehyde desorption energy is described by geometric and acid−base contributions, whereas its first C−H stripping is driven by redox and acid−base contributions. With these rules, the unique magnitude that ultimately controls selectivity, E_{TS}, can be retrieved. On the basis of the obtained equations, E_{TS} is expressed as a function of the aforementioned terms (ensemble, redox, acid−base), providing a correlation that improves the previous value obtained by means of the BEP-derived TSS relationships. The collective descriptor improves the correlation and diminishes the associated errors below 0.1 eV. This means that for a typical reaction at 500 K the error in the predicted rates is diminished by 1 order of magnitude.

The present results open a new concept for the use of linear scaling relationships to complex surfaces as oxides and polyfunctionalized molecules.

■ ASSOCIATED CONTENT

Supporting Information

Projected DOS (PDOS) of the O(2p) band corresponding to lattice oxygens of pristine and doped CeO_2(111), ensemble area descriptor, formaldehyde desorption energy (E_{des}) and activation energy (E_a) for the first C−H cleavage as a function of the five descriptors, E_a as a function of the two-variable descriptor that includes lattice parameter or M−O bond and oxygen basicity, all relative energies of Figure 2, and values for all descriptors considered in this work (PDF)

■ AUTHOR INFORMATION

Corresponding Authors

*E-mail for M.C.-C.: mcapdevila@iciq.es.

*E-mail for N.L.: nlopez@iciq.es.

Notes

The authors declare no competing financial interest.

■ ACKNOWLEDGMENTS

This research has been supported by an ERC Starting Grant (ERC-2010-StG-258406), the Ministerio de Economía y Competitividad-MINECO (CTQ2012-33826), and the Generalitat de Catalunya-AGAUR (SGR-2014-SGR-145). We acknowledge the BSC-RES for providing generous computational resources.

■ REFERENCES

(1) Nørskov, J. K.; Bligaard, T.; Rossmeisl, J.; Christensen, C. H. *Nat. Chem.* **2009**, *1*, 37−46.

(2) Nørskov, J. K.; Bligaard, T.; Hvolbæk, B.; Abild-Pedersen, F.; Chorkendorff, I.; Christensen, C. H. *Chem. Soc. Rev.* **2008**, *37*, 2163−2171.

(3) Studt, F.; Abild-Pedersen, F.; Bligaard, T.; Sørensen, R. Z.; Christensen, C. H.; Nørskov, J. K. *Science* **2008**, *320*, 1320−1322.

(4) Honkala, K.; Łodziana, Z.; Remediakis, I. N.; Lopez, N. *Top. Catal.* **2014**, *57*, 14−24.

(5) Abild-Pedersen, F.; Greeley, J.; Studt, F.; Rossmeisl, J.; Munter, T.; Moses, P.; Skúlason, E.; Bligaard, T.; Nørskov, J. *Phys. Rev. Lett.* **2007**, *99*, 016105.

(6) Fernández, E. M.; Moses, P. G.; Toftelund, A.; Hansen, H. A.; Martínez, J. I.; Abild-Pedersen, F.; Kleis, J.; Hinnemann, B.; Rossmeisl, J.; Bligaard, T.; Nørskov, J. K. *Angew. Chem., Int. Ed.* **2008**, *47*, 4683−4686.

(7) Calle-Vallejo, F.; Loffreda, D.; Koper, M. T. M.; Sautet, P. *Nat. Chem.* **2015**, *7*, 403−410.

(8) Bahn, S. R.; Lopez, N.; Nørskov, J. K.; Jacobsen, K. W. *Phys. Rev. B: Condens. Matter Mater. Phys.* **2002**, *66*, 081405.

(9) García-Muelas, R.; López, N. *J. Phys. Chem. C* **2014**, *118*, 17531−17537.

(10) Salciccioli, M.; Chen, Y.; Vlachos, D. G. *J. Phys. Chem. C* **2010**, *114*, 20155−20166.

(11) Salciccioli, M.; Edie, S. M.; Vlachos, D. G. *J. Phys. Chem. C* **2012**, *116*, 1873−1886.

(12) Ganduglia-Pirovano, M. V.; Popa, C.; Sauer, J.; Abbott, H.; Uhl, A.; Baron, M.; Stacchiola, D.; Bondarchuk, O.; Shaikhutdinov, S.; Freund, H.-J. *J. Am. Chem. Soc.* **2010**, *132*, 2345−2349.

(13) Rellán-Piñeiro, M.; López, N. *ChemSusChem* **2015**, *8*, 2231−2239.

(14) Deml, A. M.; Stevanović, V.; Muhich, C. L.; Musgrave, C. B.; O'Hayre, R. *Energy Environ. Sci.* **2014**, *7*, 1996−2004.

(15) Deml, A. M.; Holder, A. M.; O'Hayre, R. P.; Musgrave, C. B.; Stevanović, V. *J. Phys. Chem. Lett.* **2015**, *6*, 1948−1953.

(16) Bronsted, J. N. *Chem. Rev.* **1928**, *5*, 231−338.

(17) Evans, M. G.; Polanyi, M. *Trans. Faraday Soc.* **1938**, *34*, 11−24.

(18) Nørskov, J. K.; Bligaard, T.; Logadottir, A.; Bahn, S.; Hansen, L. B.; Bollinger, M.; Bengaar, H.; Hammer, B.; Sljivancanin, Z.; Mavrikakis, M.; Xu, Y.; Dahl, S.; Jacobsen, C. J. H. *J. Catal.* **2002**, *209*, 275−278.

(19) van Santen, R. A.; Neurock, M.; Shetty, S. G. *Chem. Rev.* **2010**, *110*, 2005−2048.

(20) Loffreda, D.; Delbecq, F.; Vigné, F.; Sautet, P. *Angew. Chem., Int. Ed.* **2009**, *48*, 8978−8980.

(21) Zaffran, J.; Michel, C.; Auneau, F.; Delbecq, F.; Sautet, P. *ACS Catal.* **2014**, *4*, 464−468.

(22) García-Muelas, R.; Li, Q.; López, N. *ACS Catal.* **2015**, *5*, 1027−1036.

(23) Zaffran, J.; Michel, C.; Delbecq, F.; Sautet, P. *J. Phys. Chem. C* **2015**, *119*, 12988−12998.

(24) Trovarelli, A. In *Catalysis by Ceria and Related Materials*; Trovarelli, A., Ed.; Imperial College Press: London, 2002.

(25) Nolan, M.; Parker, S. C.; Watson, G. W. *Surf. Sci.* **2005**, *595*, 223−232.

(26) Yao, H. C.; Yao, Y. F. Y. *J. Catal.* **1984**, *86*, 254−265.

(27) Fu, Q.; Saltsburg, H.; Flytzani-Stephanopoulos, M. *Science* **2003**, *301*, 935−938.

(28) Hilaire, S.; Wang, X.; Luo, T.; Gorte, R.; Wagner, J. *Appl. Catal., A* **2001**, *215*, 271−278.

(29) Yoo, J. S.; Bhattacharyya, A. A.; Radlowski, C. A. *Ind. Eng. Chem. Res.* **1991**, *30*, 1444−1448.

(30) Yoo, J. S.; Bhattacharyya, A. A.; Radlowski, C. A.; Karch, J. A. *Appl. Catal., B* **1992**, *1*, 169−189.

(31) Amrute, A. P.; Mondelli, C.; Moser, M.; Novell-Leruth, G.; López, N.; Rosenthal, D.; Farra, R.; Schuster, M. E.; Teschner, D.; Schmidt, T.; Pérez-Ramírez, J. *J. Catal.* **2012**, *286*, 287−297.

(32) Vilé, G.; Bridier, B.; Wichert, J.; Pérez-Ramírez, J. *Angew. Chem., Int. Ed.* **2012**, *51*, 8620−8623.

(33) McFarland, E. W.; Metiu, H. *Chem. Rev.* **2013**, *113*, 4391−4427.

(34) Hu, Z.; Metiu, H. *J. Phys. Chem. C* **2011**, *115*, 17898−17909.

(35) Mogensen, M.; Sammes, N. M.; Tompsett, G. A. *Solid State Ionics* **2000**, *129*, 63−94.

(36) Fu, Y.-P.; Tseng, C.-W.; Peng, P.-C. *J. Eur. Ceram. Soc.* **2008**, *28*, 85−90.

(37) Esposito, V.; Zunic, M.; Traversa, E. *Solid State Ionics* **2009**, *180*, 1069−1075.

(38) Sen, S.; Avila-Paredes, H. J.; Kim, S. *J. Mater. Chem.* **2008**, *18*, 3915−3917.

(39) Steele, B. C.; Heinzel, A. *Nature* **2001**, *414*, 345−352.

(40) Andersson, D. A.; Simak, S. I.; Skorodumova, N. V.; Abrikosov, I. A.; Johansson, B. *Proc. Natl. Acad. Sci. U. S. A.* **2006**, *103*, 3518−3521.
(41) Andersson, D.; Simak, S.; Skorodumova, N.; Abrikosov, I.; Johansson, B. *Phys. Rev. B: Condens. Matter Mater. Phys.* **2007**, *76*, 174119.
(42) Andersson, D. A.; Simak, S. I.; Skorodumova, N. V.; Abrikosov, I. A.; Johansson, B. *Appl. Phys. Lett.* **2007**, *90*, 031909.
(43) Keating, P. R. L.; Scanlon, D. O.; Watson, G. W. *J. Mater. Chem. C* **2013**, *1*, 1093−1098.
(44) Vanpoucke, D. E. P.; Bultinck, P.; Cottenier, S.; Van Speybroeck, V.; Van Driessche, I. *J. Mater. Chem. A* **2014**, *2*, 13723−13737.
(45) Murgida, G. E.; Ferrari, V.; Ganduglia-Pirovano, M. V.; Llois, A. M. *Phys. Rev. B: Condens. Matter Mater. Phys.* **2014**, *90*, 115120.
(46) Nolan, M. *J. Mater. Chem.* **2011**, *21*, 9160−9168.
(47) Yeriskin, I.; Nolan, M. *J. Chem. Phys.* **2009**, *131*, 244702.
(48) Nolan, M. *J. Phys. Chem. C* **2011**, *115*, 6671−6681.
(49) Yeriskin, I.; Nolan, M. *J. Phys.: Condens. Matter* **2010**, *22*, 135004.
(50) Vilé, G.; Dähler, P.; Vecchietti, J.; Baltanás, M.; Collins, S.; Calatayud, M.; Bonivardi, A.; Pérez-Ramírez, J. *J. Catal.* **2015**, *324*, 69−78.
(51) Kalamaras, C. M.; Dionysiou, D. D.; Efstathiou, A. M. *ACS Catal.* **2012**, *2*, 2729−2742.
(52) Kalamaras, C. M.; Petallidou, K. C.; Efstathiou, A. M. *Appl. Catal., B* **2013**, *136*−*137*, 225−238.
(53) Katta, L.; Thrimurthulu, G.; Reddy, B. M.; Muhler, M.; Grünert, W. *Catal. Sci. Technol.* **2011**, *1*, 1645−1652.
(54) Reddy, B. M.; Bharali, P.; Saikia, P.; Khan, A.; Loridant, S.; Muhler, M.; Grunert, W. *J. Phys. Chem. C* **2007**, *111*, 1878−1881.
(55) Farra, R.; García-Melchor, M.; Eichelbaum, M.; Hashagen, M.; Frandsen, W.; Allan, J.; Girgsdies, F.; Szentmiklósi, L.; López, N.; Teschner, D. *ACS Catal.* **2013**, *3*, 2256−2268.
(56) Lu, Y.-H.; Chen, H.-T. *J. Phys. Chem. C* **2014**, *118*, 10043−10052.
(57) Peng, Y.; Yu, W.; Su, W.; Huang, X.; Li, J. *Catal. Today* **2015**, *242*, 300−307.
(58) Sharma, S.; Hu, Z.; Zhang, P.; McFarland, E. W.; Metiu, H. *J. Catal.* **2011**, *278*, 297−309.
(59) Upham, D. C.; Derk, A. R.; Sharma, S.; Metiu, H.; McFarland, E. W. *Catal. Sci. Technol.* **2015**, *5*, 1783−1791.
(60) Derk, A. R.; Moore, G. M.; Sharma, S.; McFarland, E. W.; Metiu, H. *Top. Catal.* **2014**, *57*, 118−124.
(61) Tatibouët, J. M. *Appl. Catal., A* **1997**, *148*, 213−252.
(62) Badlani, M.; Wachs, I. E. *Catal. Lett.* **2001**, *75*, 137−149.
(63) Mullins, D. R.; Robbins, M. D.; Zhou, J. *Surf. Sci.* **2006**, *600*, 1547−1558.
(64) Albrecht, P. M.; Mullins, D. R. *Langmuir* **2013**, *29*, 4559−4567.
(65) Capdevila-Cortada, M.; García-Melchor, M.; López, N. *J. Catal.* **2015**, *327*, 58−64.
(66) Kresse, G. *Phys. Rev. B: Condens. Matter Mater. Phys.* **1996**, *54*, 11169−11186.
(67) Kresse, G.; Furthmüller, J. *Comput. Mater. Sci.* **1996**, *6*, 15−50.
(68) Perdew, J. P.; Burke, K.; Ernzerhof, M. *Phys. Rev. Lett.* **1996**, *77*, 3865−3868.
(69) Dudarev, S. L.; Savrasov, S. Y.; Humphreys, C. J.; Sutton, A. P. *Phys. Rev. B: Condens. Matter Mater. Phys.* **1998**, *57*, 1505−1509.
(70) Fabris, S.; de Gironcoli, S.; Baroni, S.; Vicario, G.; Balducci, G. *Phys. Rev. B: Condens. Matter Mater. Phys.* **2005**, *72*, 237102.
(71) Ganduglia-Pirovano, M.; Da Silva, J.; Sauer, J. *Phys. Rev. Lett.* **2009**, *102*, 026101.
(72) García-Melchor, M.; López, N. *J. Phys. Chem. C* **2014**, *118*, 10921−10926.
(73) Blöchl, P. E. *Phys. Rev. B: Condens. Matter Mater. Phys.* **1994**, *50*, 17953−17979.
(74) Kümmerle, E.; Heger, G. *J. Solid State Chem.* **1999**, *147*, 485−500.
(75) Da Silva, J.; Ganduglia-Pirovano, M.; Sauer, J.; Bayer, V.; Kresse, G. *Phys. Rev. B: Condens. Matter Mater. Phys.* **2007**, *75*, 045121.
(76) Henkelman, G.; Uberuaga, B. P.; Jónsson, H. *J. Chem. Phys.* **2000**, *113*, 9901−9904.
(77) Henkelman, G.; Jónsson, H. *J. Chem. Phys.* **1999**, *111*, 7010−7022.
(78) Kropp, T.; Paier, J. *J. Phys. Chem. C* **2014**, *118*, 23690−23700.
(79) Kropp, T.; Paier, J.; Sauer, J. *J. Am. Chem. Soc.* **2014**, *136*, 14616−14625.
(80) Döbler, J.; Pritzsche, M.; Sauer, J. *J. Am. Chem. Soc.* **2005**, *127*, 10861−10868.
(81) Hammer, B.; Nørskov, J. K. In *Chemisorption and Reactivity on Supported Clusters and Thin Films*; Lambert, R. M., Pacchioni, G., Eds.; Springer Netherlands: Dordrecht, The Netherlands, 1997; pp 285−351.
(82) Hammer, B.; Morikawa, Y.; Nørskov, J. K. *Phys. Rev. Lett.* **1996**, *76*, 2141−2144.
(83) Grasselli, R. K. *Top. Catal.* **2002**, *21*, 79−88.
(84) The electron added was localized on a single Ce(III) cation. Charge compensation is applied on these non-neutral unit cells by the addition of a homogeneous background charge. This is sensitive to the vacuum width, which can however be considered as constant for our study.
(85) Bansode, A.; Urakawa, A. *ACS Catal.* **2014**, *4*, 3877−3880.
(86) O'Brien, M. G.; Beale, A. M.; Jacques, S. D. M.; Buslaps, T.; Honkimaki, V.; Weckhuysen, B. M. *J. Phys. Chem. C* **2009**, *113*, 4890−4897.
(87) Bowker, M.; Carley, A. F.; House, M. *Catal. Lett.* **2008**, *120*, 34−39.
(88) Mavrikakis, M.; Hammer, B.; Nørskov, J. *Phys. Rev. Lett.* **1998**, *81*, 2819−2822.
(89) Childers, D. J.; Schweitzer, N. M.; Shahri, S. M. K.; Rioux, R. M.; Miller, J. T.; Meyer, R. J. *Catal. Sci. Technol.* **2014**, *4*, 4366−4377.
(90) Metiu, H.; Chrétien, S.; Hu, Z.; Li, B.; Sun, X. *J. Phys. Chem. C* **2012**, *116*, 10439−10450.
(91) Torres, D.; Lopez, N.; Illas, F.; Lambert, R. M. *Angew. Chem., Int. Ed.* **2007**, *46*, 2055−2058.
(92) Farra, R.; Wrabetz, S.; Schuster, M. E.; Stotz, E.; Hamilton, N. G.; Amrute, A. P.; Pérez-Ramírez, J.; López, N.; Teschner, D. *Phys. Chem. Chem. Phys.* **2013**, *15*, 3454−3465.
(93) Reddy, B. M. In *Metal Oxides: Chemistry and Applications*; Fierro, J. L. G., Ed.; CRC Press: Boca Raton, FL, 2005; pp 215−237.